

## Ductility loss in Hydrogen-charged Ductile Cast Iron

**Hisao Matsunaga<sup>1, 2, 3, 4, \*</sup>, Teruki Usuda<sup>5</sup>, Keiji Yanase<sup>4, 6</sup>, Masahiro Endo<sup>4, 6</sup>**

<sup>1</sup> Department of Mechanical Engineering, Kyushu University, Fukuoka 819-0395, Japan

<sup>2</sup> International Institute for Carbon-Neutral Energy Research (I2CNER), Kyushu University, Fukuoka 819-0395, Japan

<sup>3</sup> Research Center for Hydrogen Industrial Use and Storage (HYDROGENIUS), Kyushu University

<sup>4</sup> Institute of Materials Science and Technology, Fukuoka University, Fukuoka 814-0180, Japan

<sup>5</sup> Graduate School of Fukuoka University, Fukuoka 814-0180, Japan

<sup>6</sup> Department of Mechanical Engineering, Fukuoka University, Fukuoka 814-0180, Japan

\* Corresponding author: matsunaga@mech.kyushu-u.ac.jp

---

**Abstract** Hydrogen-induced ductility loss in ductile cast iron (DCI) was studied by conducting a series of tensile tests with three different crosshead speeds. By utilizing the thermal desorption spectroscopy and the hydrogen microprint technique, it was found that most of the solute hydrogen was diffusive and mainly segregated at the graphite, graphite/matrix interface zone and the cementite of pearlite in the matrix. The fracture process of the non-charged specimen was dominated by the ductile dimple fracture, whereas that of the hydrogen-charged specimen became less ductile by accompanying the interconnecting cracks between the adjacent graphite nodules. Inside of the hydrogen-charged specimen, the interspaces generated by the interfacial debonding between graphite and matrix are filled with hydrogen gas in the early stage of the fracture process. In the subsequent fracture process, such a local hydrogen gas atmosphere coupled with a stress-induced diffusion attracts hydrogen to the crack tip, which results in a time-dependent ductility loss.

**Keywords** Hydrogen, Hydrogen embrittlement, Ductile cast iron, Ductility loss

---

### 1. Introduction

Ductile cast iron (DCI) is widely used for pipes in city gas pipelines and is a prospective candidate material for hydrogen gas pipes. However, to the authors' knowledge, there exist few studies about the effect of hydrogen on the strength properties of cast irons. On the other hand, with respect to the hydrogen-induced ductility loss in the ferritic or ferritic-pearlitic steels (*e.g.* carbon steels), a number of studies have examined the degradation process in the tensile properties [1-8]. These studies clarified that the ductility loss was mainly attributed to the hydrogen-induced acceleration of the fracture process (*e.g.* nucleation of voids or cracks and their subsequent growth). In addition to the ferritic-pearlitic matrix, DCI contains numerous spheroidal graphites, which can serve not only as stress-concentration sites but also as hydrogen-trap sites. Therefore, the process of hydrogen-induced degradation in cast iron, if any, could be more complex than carbon steels due to the presence of graphites. In this study, as a first attempt to understand the hydrogen effect on the various strength properties of DCI, our focus is primarily on the ductility loss due to internal hydrogen. A unique degradation process associated with solute hydrogen behavior is demonstrated and discussed based on the observations of the fracture process and the microscopic hydrogen segregation behavior.

### 2. Material and experimental methods

#### 2.1. Material and specimen

The test specimens were cut out from a ductile cast iron pipe that was produced by centrifugal casting. The chemical composition in mass% was 3.70 C, 1.78 Si, 0.34 Mn, 0.058 P, 0.007 S and bal.

Fe. The microstructure was composed of a ferrite/pearlite matrix in conjunction with spheroidal graphites. The volume fraction of each phase, which was measured at a mirror-finished section, was 21 % for pearlite, 15 % for graphite and bal. ferrite. The average value of the Vickers hardness,  $HV$ , measured with a load of 9.8 N, was 169 in the ferrite section and 217 in the pearlite section. The round bar specimens, having a diameter of 5 mm and a gage length of 30 mm, were used for the tensile tests. The surface of the specimen was finished by polishing with emery papers and then by buffing with an alumina paste.

## 2.2. Hydrogen-charging, TDS analysis and microscopic visualization of solute hydrogen

The specimens were charged with hydrogen by soaking them in an aqueous solution of 20 mass% ammonium thiocyanate at 313 K for 48 hours. The hydrogen-charged specimens were re-polished before tensile tests to remove the corrosion layer produced by the charging. A number of studies (*cf.* [9-12]) have reported that cast irons as well as steels are vulnerable to surface cracking due to hydrogen-charging. To confirm the presence or absence of a crack in the specimen after the charging, the surface was mirror-polished with buff and then etched with nital. In this study, no crack was detected on the specimen surface.

The hydrogen content in the specimens was measured by the thermal desorption spectroscopy (TDS). Circular disks of 0.8 mm-thick were sliced from the specimen cross section and used for the TDS analysis. The measurements were carried out up to a temperature of 873 K (600 °C) at a heating rate of 0.5 K/s.

The hydrogen emission from the cast iron was visualized by using the hydrogen microprint technique (HMT) [13-15].

## 2.3. Tensile test

Displacement controlled tests were carried out with three different crosshead speeds (CHSs) of 50, 1 and 0.02 mm/min by using a hydraulically-controlled testing machine in ambient air. By assuming that crosshead displacement is equal to the elongation of the test section, the strain rate  $\dot{\epsilon}$  for each CHS is rendered as  $2.8 \times 10^{-2}$ ,  $5.6 \times 10^{-4}$  and  $1.1 \times 10^{-5} \text{ s}^{-1}$ , respectively. During the experiment, strain was measured with a clip gauge extensometer.

# 3. Results and discussion

## 3.1. Hydrogen content in specimen and the desorption behavior

Figure 1 displays the residual hydrogen content,  $C_{H, R}$ , as a function of the total hold time after hydrogen-charging,  $\Delta t$ . The content decreased gradually while the charged specimen was exposed to ambient air. After 200 hours, the content reduced to the same level of hydrogen content as in the non-charged specimen. From the reduction of hydrogen content, an apparent hydrogen diffusion coefficient at room temperature,  $D'$ , was estimated by means of Demarez *et al.*'s solution for the hydrogen diffusion from a finite cylinder [16]. The least-square fitting rendered the coefficient to be  $D' = 9.1 \times 10^{-13} \text{ m}^2/\text{s}$ , which is relatively smaller than the diffusion coefficient in steels. In the hydrogen-charged specimens, all the tensile tests were initiated within 2 hours after hydrogen-charging, and they were finished within 3 hours after the initiation of the test; *i.e.* around 3-5 mass ppm of hydrogen seemed to be present in the specimen during the tensile test.

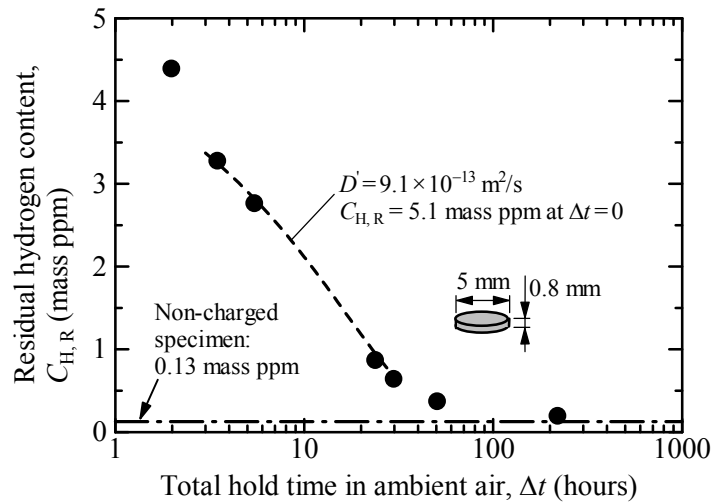
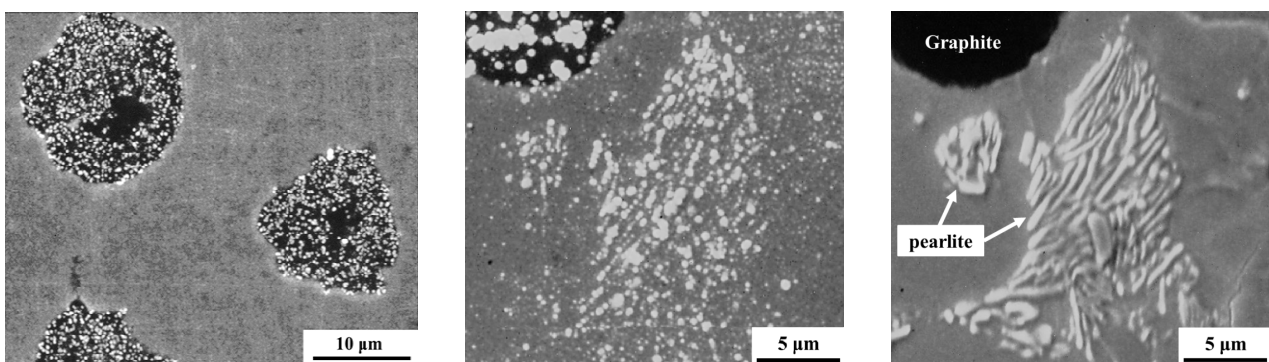


Figure 1. Residual hydrogen content as a function of total hold time in ambient air (Broken line shows the least-square fitting with Demarez et al.'s solution for the hydrogen diffusion from a finite cylinder [16])

### 3.2. Hydrogen segregation in microstructure

Figure 2 shows the result of HMT observation on a longitudinal section of a hydrogen-charged specimen. Numerous white spots in the photographs represent the silver particles to which the silver bromide particles were reduced by emitted hydrogen. The silver particles were mainly observed at the cross section of graphite nodules as exhibited in Figure 2(a). The particles were also observed along the cementite lamellae in pearlite colonies as shown in Figure 2(b), but were barely observed at ferrite. It is noted that in the non-charged specimens, no hydrogen emission was detected by the HMT.

Figure 3 shows the HMT images on the fracture surface of the hydrogen-charged specimen. The HMT was applied right after the tensile test. As shown, hydrogen emission was observed not only at the graphite nodules, but also at the concaves apart from the graphite nodules. This result implies that a great amount of hydrogen exists at or near the graphite/matrix interface as well as in the graphite itself.



(a) Hydrogen emission from graphite (b) Hydrogen emission from pearlite, HMT image (left); Etched microstructure at the same area (right)

Figure 2. HMT images on a longitudinal section of the hydrogen-charged specimen

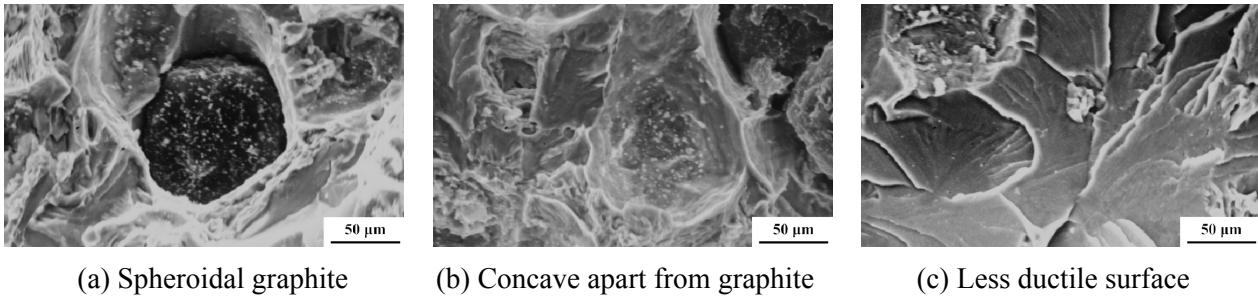


Figure 3. HMT images on the fracture surface of the hydrogen-charged specimen  
(Crosshead speed: 1.0 mm/min)

### 3.3. Results of tensile testing under different CHSs

Figure 4 displays the engineering stress-strain curves. As demonstrated, hydrogen-charging markedly reduced the percentage elongation after fracture. In addition, Figure 5 illustrates the relationship between the percentage reduction of area (%RA) and CHS. For the sake of more general illustration of the experimental data, the approximated scale of strain rate,  $\dot{\epsilon}$ , is additionally indicated on the top of the figure. It is noted that the strain rate was calculated by the CHS divided by the gage length of the specimen. In the non-charged specimen, %RA was nearly constant irrespective of CHS. On the other hand, in the hydrogen-charged specimen, %RA was gradually reduced with a decrease in CHS, *i.e.* a strain-rate-dependent ductility loss was manifested.

### 3.4. Fracture process

Figure 6 shows the SEM micrographs at the central part of fracture surfaces, and the non-charged (left-hand side) and the hydrogen-charged (right-hand side) specimens are compared. In the non-charged specimens, the ductile fracture with dimples was dominantly observed regardless of CHS. In the hydrogen-charged specimen tested at a CHS of 50 mm/min, the ductile dimple fracture was still dominant, but a small fraction of less ductile fracture appeared. In contrast, in the hydrogen-charged specimen tested at a CHS of 0.02 mm/min, the fracture morphology apparently became much less ductile.

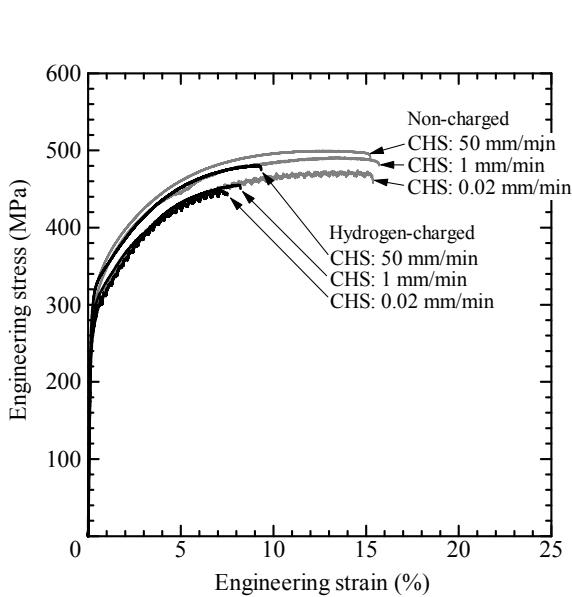


Figure 4. Engineering stress-strain curves

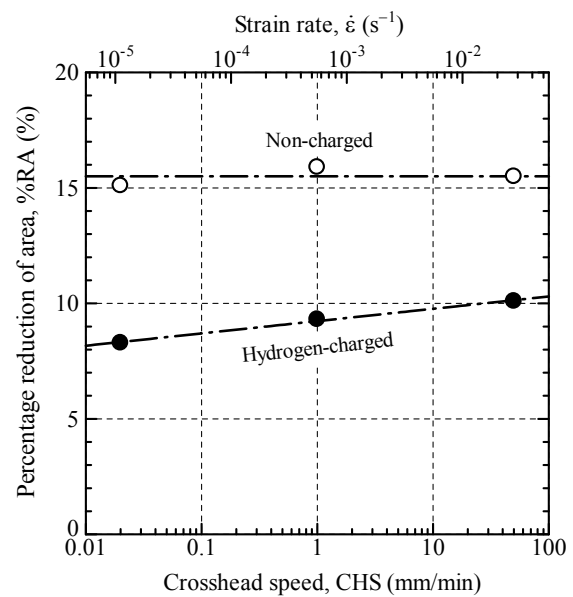
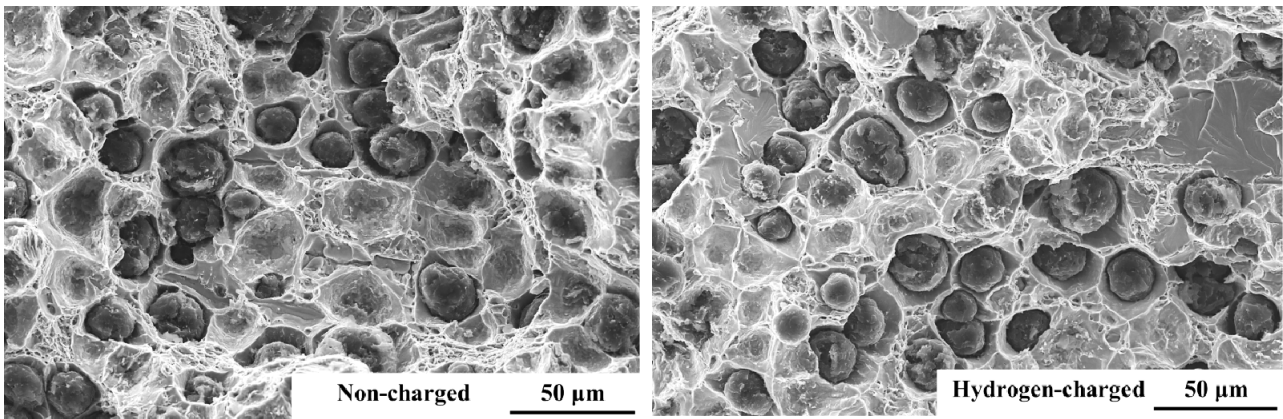
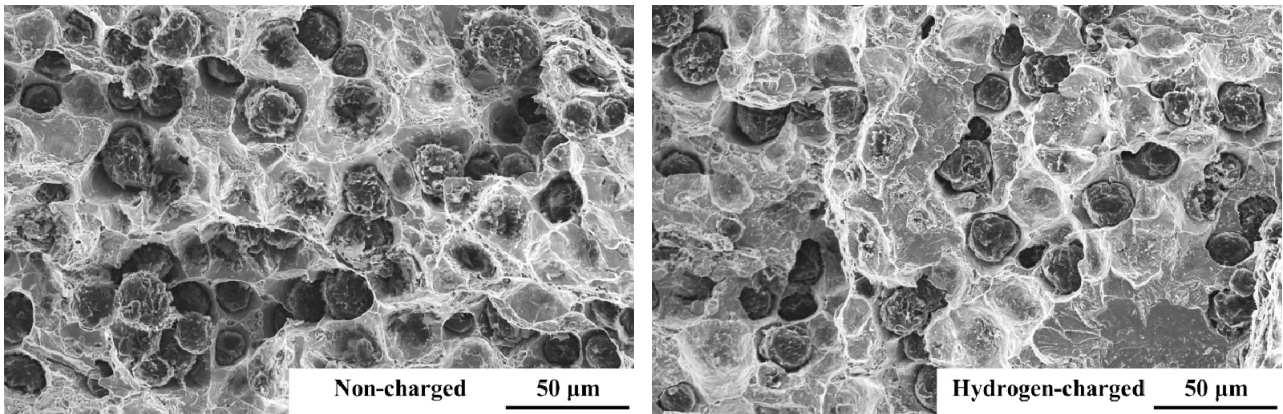


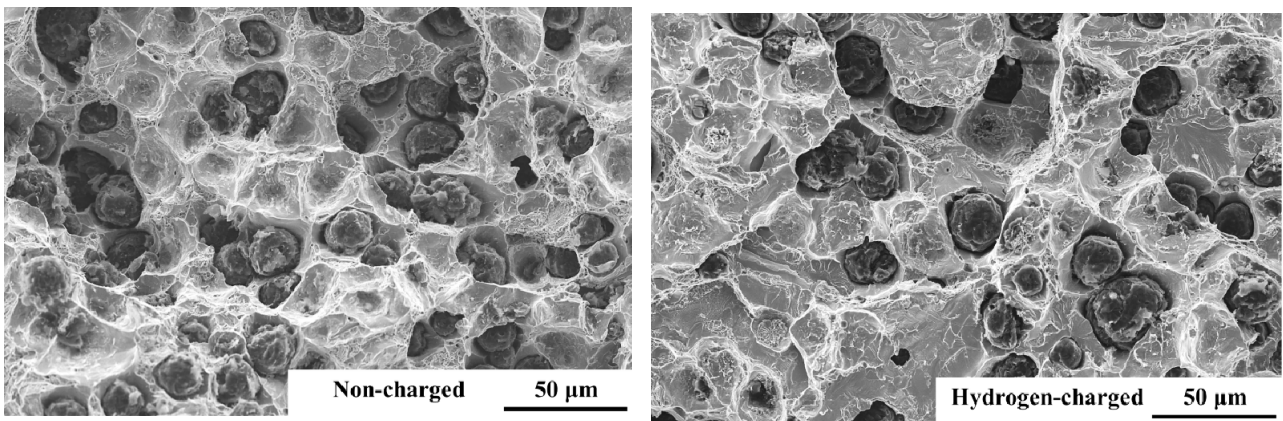
Figure 5. Relationship between the percentage reduction of area and the crosshead speed



(a) CHS: 50 mm/min ( $\dot{\epsilon} \approx 2.8 \times 10^{-2} \text{ s}^{-1}$ )



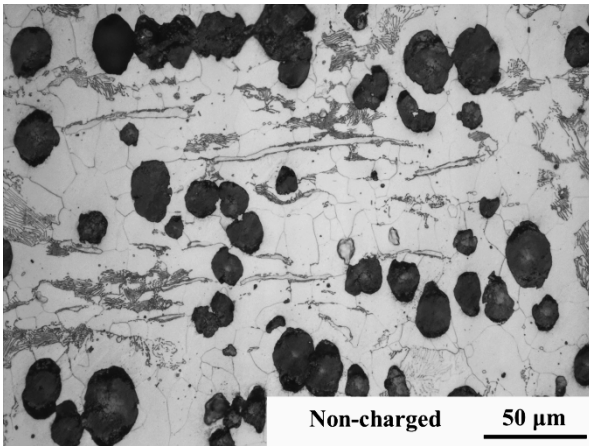
(b) CHS: 1 mm/min ( $\dot{\epsilon} \approx 5.6 \times 10^{-4} \text{ s}^{-1}$ )



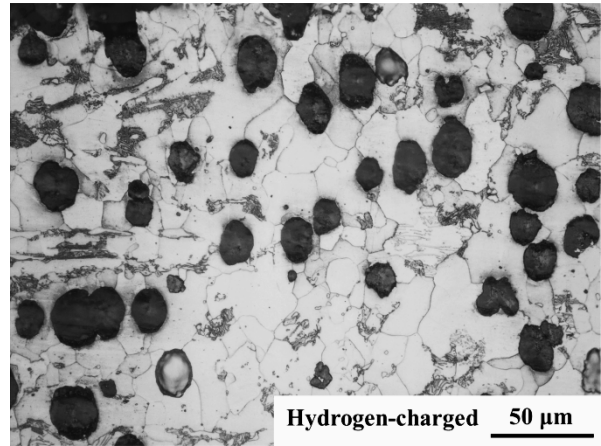
(c) CHS: 0.02 mm/min ( $\dot{\epsilon} \approx 1.1 \times 10^{-5} \text{ s}^{-1}$ )

Figure 6. SEM micrographs at the central part of the fracture surfaces (CHS: Crosshead speed)

↕ Loading axis

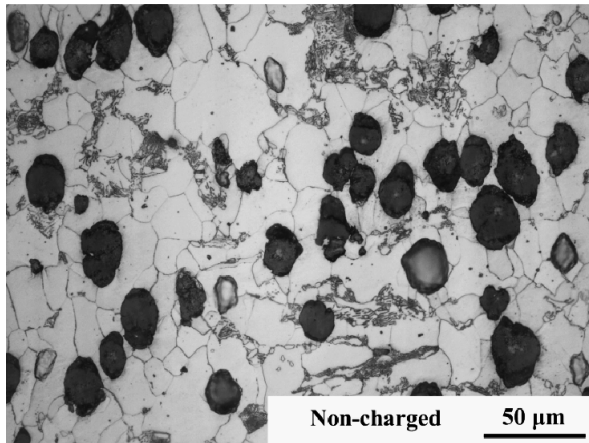


↕ Loading axis

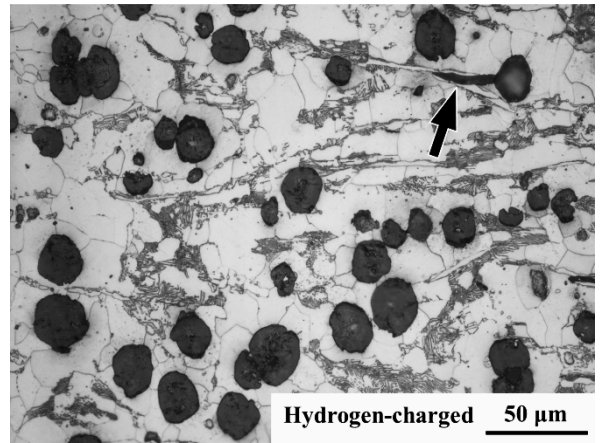


(a) CHS: 50 mm/min ( $\dot{\epsilon} \approx 2.8 \times 10^{-2} \text{ s}^{-1}$ )

↕ Loading axis

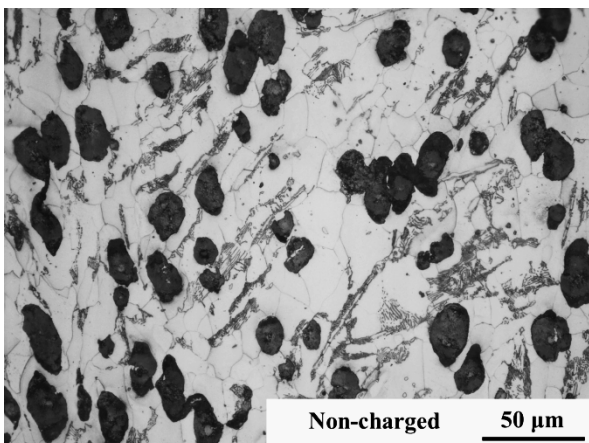


↕ Loading axis

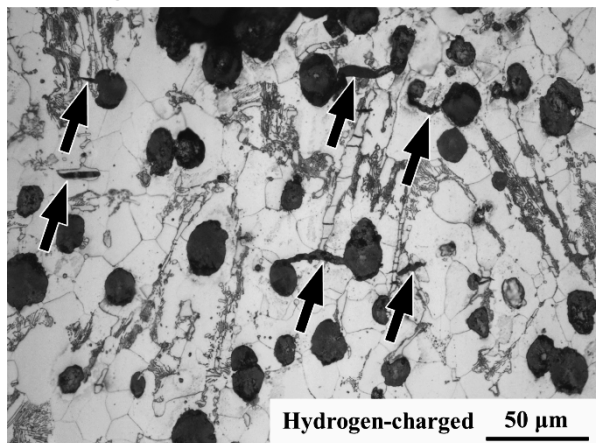


(b) CHS: 1 mm/min ( $\dot{\epsilon} \approx 5.6 \times 10^{-4} \text{ s}^{-1}$ )

↕ Loading axis



↕ Loading axis

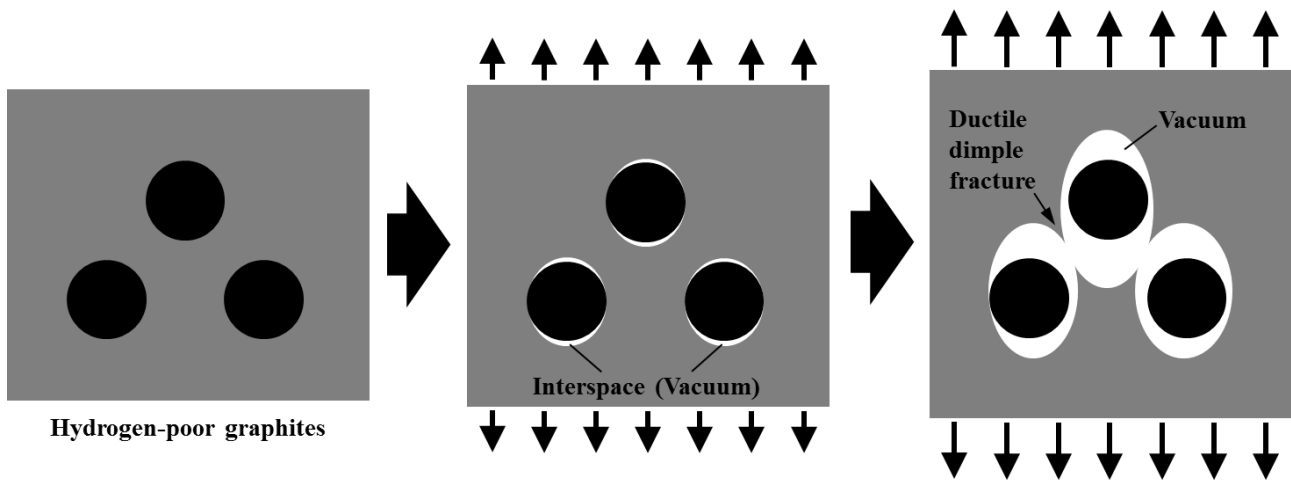


(c) CHS: 0.02 mm/min ( $\dot{\epsilon} \approx 1.1 \times 10^{-5} \text{ s}^{-1}$ )

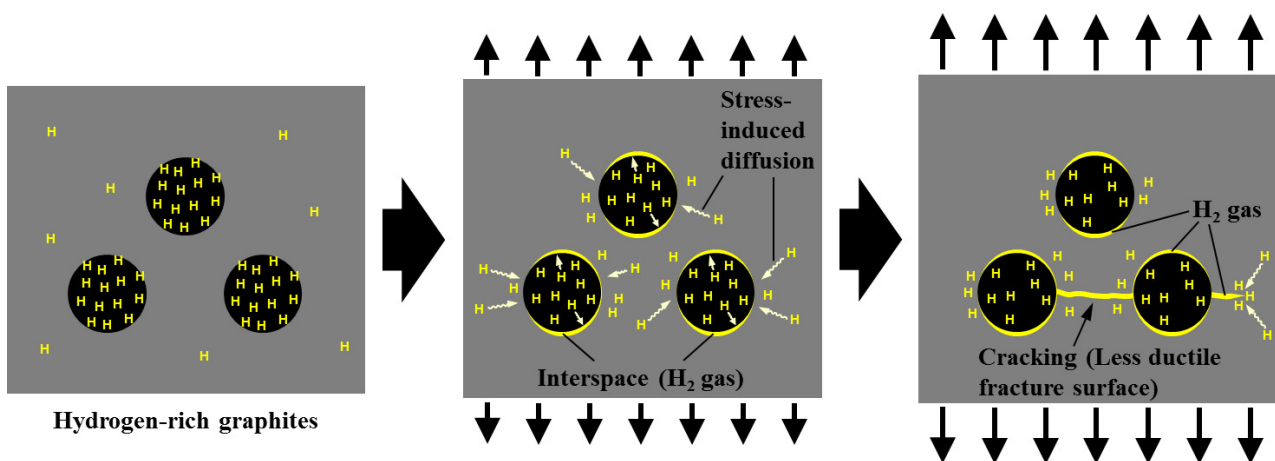
Figure 7. Fracture morphology on the etched cross sections just beneath the fracture surfaces (Arrows indicate interconnecting cracks. CHS: Crosshead speed)

Figure 7 exhibits the fracture morphology on the etched cross sections just beneath the fracture surfaces. In the non-charged specimens (left-hand side), most of the graphites coalesced with each other leading to a typical ductile behavior, regardless of CHS. On the other hand, in the hydrogen-charged specimens (right-hand side), the fracture process was accompanied with the interconnecting cracks between adjacent graphites. This tendency appeared prominently at lower CHS (*cf.* Figure 7(c)).

Figure 8 illustrates two distinct fracture modes in the non-charged and the hydrogen-charged specimens, which were based on the observation of fracture processes. As illustrated for the hydrogen-charged specimen, in the presence of the interconnecting cracks between graphites, less graphite nodules tend to appear on the fracture surface.



(a) Ductile dimple fracture (Non-charged specimen)



(b) Cracking in local hydrogen gas environment (Hydrogen-charged specimen)

Figure 8. Two typical fracture processes in the non-charged and the hydrogen-charged specimens

### 3.5. Influencing factors for degradation

Considering the hydrogen segregation and fracture process together with the strain-rate-dependent degradation in the hydrogen-charged specimen, it is possible to postulate the role of graphite in the degradation process as follows. In the deformation process of the non-charged specimen, an interspace generated by interfacial debonding between graphite and matrix maintains a vacuum environment. In this case, the surrounding matrix material can be relatively ductile; thereby, the fracture surface exhibits the dimple fracture accompanied with the interconnection of graphites (*cf.* Figure 8(a)). On the other hand, in the hydrogen-charged specimen, a great amount of hydrogen exists at or near the graphite/matrix interface zone, as illustrated by Figures 2 and 3. Therefore, in the early stage of the fracture process, the interspace between graphite and matrix is immediately filled with hydrogen gas (*cf.* Figure 8(b)). It is noted that the hydrogen in the interspace is of molecular in nature. Then, a certain amount of hydrogen as atom can spread into the surrounding matrix near the graphite nodule. Simultaneously, the stress-induced hydrogen diffusion inside the matrix can also contribute to increase the hydrogen concentration near the graphite. It has been shown that solute hydrogen enhances a localization of plasticity [17, 18], which hinders the formation of ductile dimple by facilitating the cracking [5-7, 17]. After the crack initiation from a graphite nodule, hydrogen is incessantly outgassed from the inside of the graphite nodule and supplied to the crack tip via the local hydrogen gas environment. The stress-induced hydrogen diffusion can also attract a certain amount of hydrogen to the crack tip. Such a process results in the localization of plasticity at the crack tip and thereby facilitates the crack growth [17]. As a consequence, smaller CHS enables more hydrogen to be concentrated to the crack tip. This time-dependent process causes the ductility loss associated with a decrease in CHS only for the hydrogen-charged specimen.

As was discussed, the DCI possesses the unique characteristics regarding the influence of hydrogen. Therefore, for proper evaluation of the hydrogen-induced degradation in DCI, the pivotal role of graphites as a *local hydrogen supplier* should be taken into consideration.

## 4. Conclusions

The effect of hydrogen-charging on ductility loss in the ductile cast iron (DCI) was investigated by conducting a series of tensile tests with three different crosshead speeds (CHSs). According to the present study, the following conclusions were obtained:

- (1) Hydrogen-charging led to a marked decrease in the percentage reduction of area (%RA). In the non-charged specimens, %RA was nearly constant irrespective of CHS, whereas in the hydrogen-charged specimens, %RA was reduced with a decrease in CHS.
- (2) Thermal desorption spectroscopy (TDS) and the hydrogen microprint technique (HMT) revealed that most of solute hydrogen in the hydrogen-charged specimen was diffusive, and they were mainly segregated at the graphite, graphite/matrix interface zone and the cementite of pearlite.
- (3) Hydrogen-charging accelerated the coalescence of graphites during the fracture process. In the non-charged specimen, the fracture process involved the ductile dimple fracture associated with the coalescence of neighboring graphites. On the other hand, in the hydrogen-charged specimen, the fracture process involved interconnecting cracks between neighboring graphites, which appeared prominently at lower CHS.
- (4) The variation in fracture morphology is attributed to a great amount of hydrogen stored in the

graphite and graphite/matrix interface zone. In the early stage of the fracture process in the hydrogen-charged specimen, the interspace generated by interfacial debonding between graphite and matrix is filled with hydrogen gas, which hinders the formation of ductile dimple by facilitating the cracking. Even in the subsequent fracture process, hydrogen is incessantly emitted from graphites. Such a local hydrogen gas atmosphere coupled with a stress-induced hydrogen diffusion inside the material attracts hydrogen to the crack tip. Accordingly, the delayed hydrogen supply causes the time-dependent degradation. To evaluate the hydrogen-induced degradation in DCI, the pivotal role of graphite as a *local hydrogen supplier* should be taken into consideration.

### Acknowledgements

The authors gratefully acknowledge Mr. Kenshin Matsuno of ShinMaywa Industries, Ltd. and Mr. Kazuhisa Hatakeyama of National Institute of Advanced Industrial Science and Technology (AIST) for their support in the experimental work. This research has been supported in part by:

- (1) The International Institute for Carbon-Neutral Energy Research (WPI-I2CNER), sponsored by the Japanese Ministry of Education, Culture, Sport, Science and Technology.
- (2) The NEDO, Fundamental Research Project on Advanced Hydrogen Science (2006 to 2012).

### References

- [1] R. Garber, I.M. Bernstein, A.W. Thompson, Effect of hydrogen on ductile fracture of spheroidized steel. *Scripta Metallurgica*, 10 (1976) 341-345.
- [2] H. Cialone, R.J. Asaro, The role of hydrogen in the ductile fracture of plain carbon steels. *Metallurgical and Materials Transactions A*, 10 (1979) 367-375.
- [3] H. Cialone, R.J. Asaro, Hydrogen assisted fracture of spheroidized plain carbon steels. *Metallurgical and Materials Transactions A*, 12 (1981) 1373-1387.
- [4] S.P. Lynch, Environmentally assisted cracking: Overview of evidence for an adsorption-induced localised-slip process. *Acta Metallurgica*, 36 (1988) 2639-2661.
- [5] H. Nishiguchi, Y. Fukushima, S. Matsuoka S, Y. Murakami, Effects of hydrogen and pre-strain on tensile properties of carbon steel STPG 370 (0.19C-0.21Si-0.56Mn, mass%) for 1 MPa hydrogen gas pipelines. *Transactions of the Japan Society of Mechanical Engineers A*, 74 (2008) 1016-1025.
- [6] H. Nishiguchi, Y. Fukushima, S. Matsuoka, Y. Murakami, Effects of hydrogen on tensile properties of ferritic-pearlitic carbon steels. *Transactions of the Japan Society of Mechanical Engineers A*, 76 (2010) 1459-1468.
- [7] T. Matsuo, N. Homma, S. Matsuoka, Y. Murakami, Effect of hydrogen and prestrain on tensile properties of carbon steel SGP (0.078C-0.012Si-0.35Mn, mass%) for 0.1MPa hydrogen pipelines. *Transactions of the Japan Society of Mechanical Engineers A*, 74 (2008) 1164-1173.
- [8] K. Yokogawa, S. Fukuyama, K. Kudo, Tensile fracture surfaces of carbon steels in high pressure hydrogen in room temperature. *Journal of the Japan Institute of Metals*, 44 (1980) 870-875.
- [9] K. Ogi, H. Hagi, A. Tahara, A. Sawamoto, H. Ikeda, Y. Hayashi, Behavior of hydrogen in ferritic spheroidal graphite cast iron with heavy section. *Journal of Japan Foundry Engineering Society*, 64 (1992) 186-191.
- [10] A. Sawamoto, Y. Hayashi, N. Ohtani, *Journal of the Japan Institute of Metals*, 43 (1979) 513-519.

- [11] T. Sakai, H. Kaji, Nucleation and growth of bubbles formed by hydrogen attack in carbon and low alloy steels. *Tetsu-to-Hagané*, 64 (1978) 430-438.
- [12] S. Nomura, M. Hasegawa, Effect of cementite distribution in low carbon steel on hydrogen attack. *Tetsu-to-Hagané*, 61 (1975) 2579-2588.
- [13] J. Ovejero-García, Hydrogen microprint technique in the study of hydrogen in steels. *Journal of Materials Science*, 20 (1985) 2623-2629.
- [14] K. Ichitani, M. Kanno, Visualization of hydrogen diffusion in steels by high sensitivity hydrogen microprint technique. *Science and Technology of Advanced Materials*, 4 (2003) 545-551.
- [15] H. Matsunaga, H. Noda, Visualization of hydrogen diffusion in a hydrogen-enhanced fatigue crack growth in type 304 stainless steel. *Metallurgical and Materials Transactions A*, 42 (2011) 2696-2705.
- [16] A. Demarez, A.G. Hocks, Meuniers FA. Diffusion of hydrogen in mild steel. *Acta Metallurgica*, 2 (1954) 214-223.
- [17] C.D. Beachem, A new model for hydrogen-assisted cracking (hydrogen “embrittlement”). *Metallurgical and Materials Transactions B*, 3 (1972) 441-455.
- [18] H.K. Birnbaum, P. Sofronis, Hydrogen-enhanced Localized Plasticity — A Mechanism for Hydrogen-related Fracture. *Materials Science and Engineering: A*, 176 (1994) 191-202.